

Tropical and Subtropical North Atlantic Vertical Wind Shear and Seasonal Tropical Cyclone Activity

JHORDANNE J. JONES, MICHAEL M. BELL, AND PHILIP J. KLOTZBACH

Department of Atmospheric Science, Colorado State University, Fort Collins, Colorado

(Manuscript received 2 July 2019, in final form 30 March 2020)

ABSTRACT

Given recent insights into the role of anticyclonic Rossby wave breaking (AWB) in driving subseasonal and seasonal North Atlantic tropical cyclone (TC) activity, this study further examines tropical versus subtropical impacts on TC activity by considering large-scale influences on boreal summer tropical zonal vertical wind shear (VWS) variability, a key predictor of seasonal TC activity. Through an empirical orthogonal function analysis, it is shown that subtropical AWB activity drives the second mode of variability in tropical zonal VWS, while El Niño–Southern Oscillation (ENSO) primarily drives the leading mode of variability. Linear regressions of the four leading principal components against tropical North Atlantic zonal VWS and accumulated cyclone energy show that while the leading mode holds much of the regression strength, some improvement can be achieved with the addition of the second and third modes. Furthermore, an index of AWB-associated VWS anomalies, a proxy for AWB impacts on the large-scale environment, may be a better indicator of summertime VWS anomalies. The utilization of this index may be used to better understand AWB's contribution to seasonal TC activity.

1. Introduction

While forecast schemes predicting North Atlantic basin seasonal tropical cyclone (TC) activity have skill (Klotzbach et al. 2017), there remain gaps in our current understanding of the large-scale mechanisms that influence the overall activity within the ocean basin. A key influence on TC activity is vertical wind shear (VWS), which acts to disrupt the TC circulation and reduce overall activity (Nolan and McGauley 2012). Until recently, the scientific literature indicated that the drivers of VWS on seasonal time scales were predominantly tropical in origin with El Niño–Southern Oscillation (ENSO) being one of the leading drivers of interannual zonal VWS variability within the tropical North Atlantic (Goldenberg and Shapiro 1996; Wang 2004; Aiyer and Thorncroft 2006). However, extratropical sources of shear resulting from Rossby wave breaking (RWB) have recently been identified as an important dynamical influence on TC activity (Zhang et al. 2016; Papin et al. 2020). In this study, we examine the physical drivers of VWS variability in the tropical North Atlantic, with the aim of improving our understanding of both tropical

and extratropical sources of VWS and their impacts on TC activity.

A common mechanism proposed for ENSO forcing of the Atlantic tropical circulation is through its modulation of the Walker circulation over the Pacific and North Atlantic basins (Wang 2004). Anomalously warm SSTs in the equatorial central and eastern Pacific associated with El Niño result in an eastward shift of the Walker circulation from the tropical western Pacific toward the international date line with associated anomalous downdrafts over the tropical Atlantic. This shift produces anomalous westerly upper-level winds and an associated increase in westerly VWS that inhibits TC development across the tropical North Atlantic main development region (MDR) (Gray 1984; Zhang et al. 2016, 2017), generally defined as the region 10°–20°N, 80°–20°W. The reverse effect occurs with an anomalously cold equatorial central and eastern Pacific (e.g., La Niña).

Atlantic SST variability is also a major driver of tropical North Atlantic VWS (Chelliah and Bell 2004; Chiang and Vimont 2004; Kossin and Vimont 2007; Klotzbach and Gray 2008). The Atlantic meridional mode (AMM) is the leading dynamical mode in tropical Atlantic climate variability, identified from a maximum covariance analysis of Atlantic sea surface temperature

Corresponding author: Jhordanne J. Jones, jhordanne.jones@colostate.edu

(SST) and 10-m winds (Chiang and Vimont 2004). The AMM is known to drive both interannual and decadal variability of vertical wind shear through its modulation of meridional gradients in SSTs and subsequent shifts in the intertropical convergence zone (ITCZ) and the Hadley circulation. A positive phase of the AMM is associated with an anomalously warm northern tropical Atlantic relative to the southern tropical Atlantic. When the AMM is positive, the ITCZ and ascending arm of the Hadley cell shift farther north, reducing upper-level westerly winds throughout the Atlantic MDR. With a negative phase of the AMM, the ascending branch of the Hadley circulation shifts farther south, increasing upper-level westerlies and thus increasing westerly shear over the MDR.

In contrast to the tropical forcing of shear by ENSO and the AMM, the midlatitude forcing arises primarily from RWB events characterized by an irreversible deformation of potential vorticity (PV) contours on an isentropic surface forced by a strong temperature or pressure gradient (McIntyre and Palmer 1983; Strong and Magnusdottir 2008; Papin et al. 2020). RWB events often result in the exchange of air between the drier midlatitudes and moister tropics via intrusions of equatorward high PV midlatitude tropospheric air and poleward low-PV tropical air (Postel and Hitchman 1999). RWB activity also shows a strong interrelationship with seasonal variations in both tropical North Atlantic VWS and TC activity (Papin et al. 2020; Zhang et al. 2017). Anticyclonic RWB (AWB) occurs more frequently in the summer than in the winter over the North Atlantic basin and has been examined in recent studies with a focus on Rossby wave breaking dynamics and their relationship with large-scale climate phenomena (Homeyer and Bowman 2013; Papin et al. 2020; Zhang et al. 2016, 2017; Zavadoff and Kirtman 2019).

Seasonal TC forecast verifications have previously highlighted the role of midlatitude interactions in suppressing TC development, such as the 2007 North Atlantic hurricane season (Klotzbach et al. 2007) and the 2013 season (Klotzbach and Gray 2013; Saunders and Lea 2014). Zhang et al. (2016) indicated that enhanced RWB frequency in 2013 was associated with strong VWS and reduced precipitable water within the North Atlantic MDR that effectively suppressed TC development. As with the 2007 hurricane season, strong suppression in 2013 occurred despite otherwise favorable environmental conditions, such as anomalously warm tropical Atlantic SSTs and a persistent ENSO-neutral phase (Klotzbach and Gray 2013). However, modulations in RWB-induced shear occur on shorter time scales than SST or ENSO, with RWB events and

their impacts typically lasting no more than a couple of days (Li et al. 2018).

Another driver of VWS and TC variability within the tropical North Atlantic is atmospheric variability closely tied to African Sahel rainfall dynamics (Landsea and Gray 1992; Aiyer and Thorncroft 2006). Earlier seasonal forecast schemes included African Sahel rainfall as a robust predictor of TC activity (Gray et al. 1994). While Sahelian rainfall variability and its impacts are not fully understood (e.g., Janicot et al. 1998, 2001), it is generally held that Sahelian rainfall has a positive correlation with North Atlantic TC activity and a negative correlation with VWS (Landsea and Gray 1992). Enhanced convection over the western Sahel results in upper-tropospheric easterly wind anomalies and a reduction of the climatological westerly shear within the North Atlantic region, promoting both TC development and intensification (Landsea and Gray 1992). Chelliah and Bell (2004) also suggest that VWS may be driven by a stationary wave response in the upper-level winds to anomalous heating from West African convection. Earlier work identified the effect of both ENSO and Sahel rainfall on the variability of the North Atlantic tropical circulation (Goldenberg and Shapiro 1996; Aiyer and Thorncroft 2006) but did not fully explore extratropical influences on the variability. Dunion (2011) highlighted that midlatitude dry-air intrusions comprised a small but significant percentage of tropical North Atlantic atmospheric soundings and suggested that dry-air intrusions from the subtropics were a persistent feature within the tropical circulation.

In the analysis that follows, we further examine the respective contributions of tropical and extratropical factors on tropical North Atlantic VWS variability. We will examine the physical drivers of tropical VWS variability in the North Atlantic and propose a way of quantifying how much extratropical AWB activity contributes to seasonal VWS. We will show that VWS anomalies associated with AWB explain a significant portion of tropical VWS variability and may lend another perspective to the predictability of the seasonal TC environment. The paper is organized as follows: section 2 outlines the data and procedures used to characterize the different drivers of VWS variability. Section 3 characterizes mean spatial VWS variability in high versus low seasons of ENSO and AWB activity. Section 4 outlines the different spatial and temporal effects of tropical versus subtropical drivers of seasonal tropical VWS anomaly. Section 5 provides a discussion of the results outlined in section 4 and summarizes the implications for improved seasonal predictions of North Atlantic TC activity.

2. Data and methods

a. Data

All atmospheric field data employed in this study are sourced from the European Centre for Medium-Range Weather Forecasts (ECMWF) interim reanalysis (ERA-Interim; [Berrisford et al. 2011](#); [Dee et al. 2011](#)). Monthly fields are gridded with a resolution of $0.75^\circ \times 0.75^\circ$ and extend from January 1979 to August 2019. Six-hourly datasets in which AWB-induced anomalies are identified are gridded with a resolution of $2.5^\circ \times 2.5^\circ$ to remove small-scale disturbances ([Postel and Hitchman 1999](#); [Zhang et al. 2016](#); [Papin et al. 2020](#)). A low-pass filtered version of the data that suppresses cycles of less than 4 months is subtracted from the original data to remove signals on longer time scales, as suggested by [Wang et al. \(2010\)](#). The seasonal cycle is then removed by subtracting the 1981–2010 monthly climatology to obtain seasonal anomaly fields.

Monthly SST anomalies from 1982 to 2016 are derived from the National Oceanic and Atmospheric Administration's Optimum Interpolation Sea Surface Temperature version 2 (NOAA OISSTv2) dataset ([Reynolds et al. 2002](#)). Monthly Sahel precipitation indices are taken from the Joint Institute of the Study of the Atmosphere and Ocean (JISAO) archive ([Mitchell 2013](#)). The analysis regions over which the climate indices are averaged are outlined in [Table 1](#).

Tropical North Atlantic VWS is defined here as the difference between the 200- and 850-hPa zonal wind fields over the region $10^\circ\text{--}30^\circ\text{N}$, $90^\circ\text{--}20^\circ\text{W}$, standardized over the period from 1981 to 2010. We have chosen to use a domain larger than the canonical MDR to ensure that the impacts of large-scale drivers are fully captured within the spatiotemporal analysis, as will be discussed further in [sections 4 and 5](#). For this study, we only utilize the zonal component of VWS as much of the observed variability in VWS is zonally modulated ([Thorncroft et al. 1993](#); [Aiyer and Thorncroft 2006](#); [Nolan and McGauley 2012](#)). Furthermore, changes in the circulation due to RWB are associated with variations in the strength and position of the subtropical upper-tropospheric westerly jet ([Homeyer and Bowman 2013](#)).

The accumulated cyclone energy (ACE) index is used to represent overall seasonal TC activity and is defined as the sum of the squares of the 6-hourly maximum wind speed for each tropical and subtropical cyclone where they at least possess 1-min maximum sustained winds of 34 kt (1 kt $\approx 0.51 \text{ m s}^{-1}$) ([Bell et al. 2000](#)). The ACE index from July–September was calculated from the National Hurricane Center's best track database (HURDAT2; [Landsea and Franklin 2013](#)). Note that we assessed VWS and AWB

TABLE 1. Regions used to define the four ENSO indices (Niño-1+2, Niño-3, Niño-3.4, and Niño-4), the African Sahel index, the anticyclonic Rossby wave breaking (AWB) index, the Atlantic meridional mode (AMM), and the Walker circulation index. All indices are standardized relative to the 1981–2010 base period.

Index	Region	Reference
Niño-1+2	$10^\circ\text{S}\text{--}0^\circ$, $90^\circ\text{--}80^\circ\text{W}$	Trenberth et al. (2020)
Niño-3	$5^\circ\text{S}\text{--}5^\circ\text{N}$, $150^\circ\text{--}90^\circ\text{W}$	Trenberth et al. (2020)
Niño-3.4	$5^\circ\text{S}\text{--}5^\circ\text{N}$, $170^\circ\text{--}120^\circ\text{W}$	Trenberth et al. (2020)
Niño-4	$5^\circ\text{S}\text{--}5^\circ\text{N}$, $160^\circ\text{E}\text{--}150^\circ\text{W}$	Trenberth et al. (2020)
Sahel	$10^\circ\text{--}20^\circ\text{N}$, $20^\circ\text{W}\text{--}10^\circ\text{E}$	Mitchell (2013)
AWB	$20^\circ\text{--}40^\circ\text{N}$, $100^\circ\text{--}5^\circ\text{W}$	Zhang et al. (2016) , Papin et al. (2020)
AMM	$21^\circ\text{S}\text{--}32^\circ\text{N}$, $74^\circ\text{W}\text{--}15^\circ\text{E}$	Zhang et al. (2016) , Chiang and Vimont (2004)
Walker index	Equatorial eastern Pacific: $5^\circ\text{S}\text{--}5^\circ\text{N}$, $160^\circ\text{--}120^\circ\text{W}$; equatorial western Pacific: $5^\circ\text{S}\text{--}5^\circ\text{N}$, $120^\circ\text{--}160^\circ\text{E}$	Wang (2004)

activity over the shorter July–September (JAS) season, in contrast to the overall hurricane season from June to November as in [Papin et al. \(2020\)](#) or July to October as in [Zhang et al. \(2017\)](#). We chose July–September as both VWS and AWB activity show distinct summertime peaks during these months. To focus on the impacts of tropical VWS, only TCs that were named south of 35°N were considered in the calculation of ACE.

b. Climate indices

[Table 1](#) presents the climate indices used to investigate the physical mechanisms driving the leading modes of tropical zonal VWS variability. Based on previous studies (e.g., [Aiyer and Thorncroft 2006](#)), we analyze the correlations with indices representing ENSO, Sahelian rainfall, the AMM, and AWB. Although the Walker circulation is closely associated with ENSO in the tropical North Atlantic atmospheric circulation, we examine it as a separate index in order to determine the extent to which it is correlated with tropical zonal VWS variability. For Atlantic SST variability, [Chiang and Vimont's \(2004\)](#) AMM index is applied. The AMM index is calculated using detrended and smoothed SSTs and low-level winds within the region $21^\circ\text{S}\text{--}32^\circ\text{N}$, $74^\circ\text{W}\text{--}15^\circ\text{E}$. Once ENSO variability is removed, a maximum covariance analysis is applied to obtain the AMM index. [Chiang and Vimont's \(2004\)](#) method is used extensively within the scientific literature ([Kossin and Vimont 2007](#); [Vimont and Kossin 2007](#)). The strength of the Pacific Walker cell is used as a proxy for the influence of the

Walker circulation over the North Atlantic region and is defined as the difference between the 500-hPa vertical velocity averaged over the equatorial eastern Pacific (5°S – 5°N , 160° – 120°W) and the equatorial western Pacific (5°S – 5°N , 120° – 160°E) (Wang 2004). All indices are standardized over 1981–2010 except for the SST indices, which are standardized over 1982–2010.

c. Detecting AWB

To detect AWB activity, we employ a simplified potential vorticity streamer (PVS) detection algorithm based on the technique outlined by Papin et al. (2020), where the PVS intensity (PVSI) index is calculated. AWB-associated PVSs are detected along the 2-PVU ($1 \text{ PVU} = 10^{-6} \text{ Km}^2 \text{s}^{-1} \text{ kg}^{-1}$) contour in the 350-K potential vorticity field using the following steps:

- The algorithm detects more than two consecutive points along the 2-PVU contour with an eastward (west to east) PV gradient ($\partial \text{PV}/\partial x > 0$) and a reversal in the poleward meridional PV gradient ($\partial \text{PV}/\partial y > 0$). This defines the upstream edge of a PV tongue. Similarly, the downstream edge may be identified with conditions ($\partial \text{PV}/\partial x < 0$) and ($\partial \text{PV}/\partial y < 0$).
- Once the points outlining the PV tongue are identified, a line connects the two end points to capture the PVS polygon and as much of the PVS area as possible. We do not assess the PVS area for a perimeter distance threshold or 3:1 aspect ratio of PV tongues as is done by Papin et al. (2020). This may lead to slight differences in the results obtained.
- The PVSI intensity is then found by calculating the standardized PV anomaly relative to a 6-hourly climatological mean integrated across all grid points within the PVS polygon and then integrated over time.
- The VWS anomaly along both the upstream and downstream edges of the detected PV tongue are collected.

For the years 1979–2016, our detection algorithm finds 32 014 AWB events in the ERA-Interim dataset. This is somewhat high when compared with the Papin et al. (2020) total of 21 149 between 1979 and 2015. However, for the July–September focus of our study, the average number of events is 337, similar to the Papin et al. (2020) value of 355 for the same season. The climatology for the total number of PV streamers detected each month (not shown) is comparable to the climatological mean intensity of AWB activity over the North Atlantic region.

Papin et al. (2020) pointed out that the detection algorithms are sensitive not only to the reanalysis dataset used, but also to the method in which the PVS area is detected. The detection method and the PVS area captured varies across studies (Postel and Hitchman 1999; Abatzoglou and Magnusdottir 2006; Wernli and

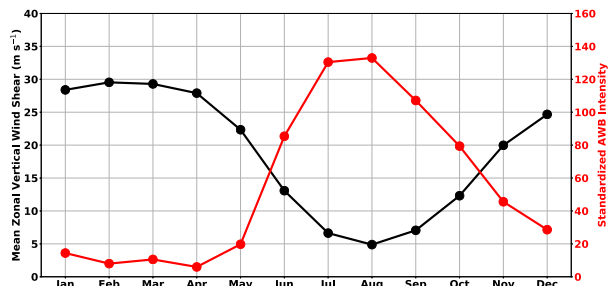


FIG. 1. 1979–2016 monthly climatology of 200–850-hPa tropical North Atlantic zonal VWS (black) and North Atlantic AWB (red). AWB is calculated as the potential vorticity streamer intensity, in which the standardized PV anomaly is integrated over the area covered by the PV streamer (Papin et al. 2020).

Sprenger 2007; Barnes and Hartmann 2012; Kunz et al. 2015). However, the AWB climatology shown in Fig. 1 is in good agreement with previous assessments of AWB variability over the North Atlantic region (Postel and Hitchman 1999; Abatzoglou and Magnusdottir 2006; Papin et al. 2020; Zhang et al. 2017). The index also correlates positively with ENSO and negatively with North Atlantic ACE. There are some differences in the years detected with above-normal or below-normal AWB activity compared with the results of both Papin et al. (2020) and Zhang et al. (2017). The differences may be due to the season chosen for our assessment. The results also show a sensitivity to the domain chosen. Similar to Zhang et al. (2017), we restrict our detection region to 20° – 40°N , 100° – 5°W , where AWB is most frequent, to better quantify the effect of AWB activity on the tropical circulation. While Zhang et al. (2017) vary the northern boundary of the detection domain, we opt to set the northern boundary at 40°N .

d. EOF analysis

To analyze the various modes of variability in tropical North Atlantic VWS, the leading empirical orthogonal functions (EOFs) are calculated via an eigenanalysis of the covariance matrix for July–September anomalous tropical North Atlantic VWS over the domain 10° – 30°N and 90° – 20°W . The VWS data are standardized prior to the EOF calculation; only the annual cycle is removed. The first four leading modes are retained for analysis as will be discussed in section 4 and are regressed against global VWS anomalies to assess possible remote versus local forcing on tropical North Atlantic VWS. The Pearson correlation coefficients between the principal components derived from the EOF analysis and the climate indices outlined in Table 1 are calculated and used to assess how large-scale subtropical forcing differs from large-scale tropical forcing of tropical North Atlantic VWS.

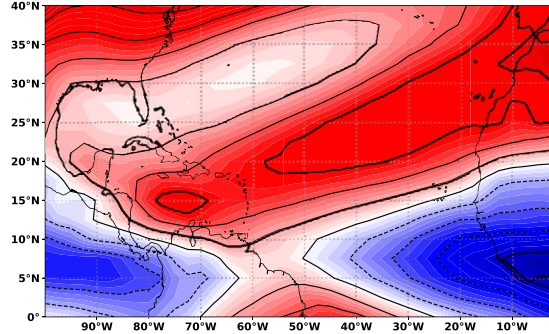


FIG. 2. July–September 1979–2016 mean zonal 200–850 hPa VWS (in m s^{-1}); black contours indicate 4 m s^{-1} intervals.

3. Tropical North Atlantic VWS variability relative to AWB

a. VWS and AWB climatology

Figure 1 shows a comparison of the 1979–2016 monthly climatology of mean zonal VWS and AWB activity over the tropical North Atlantic region. The VWS climatology (where positive values indicate westerly zonal shear and negative values indicate easterly zonal shear) exhibits maximum westerly shear in January and February. From March onward, there is a steady decline in westerly shear in conjunction with the onset of the North Atlantic hurricane season in June. This westerly shear reaches its climatological minimum in July–September, as observed in previous studies of mean shear within the North Atlantic MDR (Gray 1968; Aiyer and Thorncroft 2006). Figure 2 shows a spatial plot of the 1979–2016 July–September mean zonal VWS across the Atlantic region. There is strong mean westerly shear cutting through the North Atlantic, stretching from the Caribbean northeast to the subtropical northeastern Atlantic. The strong westerly shear is flanked by strong easterly shear south of 10°N and weaker westerly shear just north of 25°N in the western subtropical North Atlantic, similar to the observations of Gray (1968) for the mean boreal summer shear.

Collocated with the peak weakening of westerly shear during July–September is a peak occurrence in North Atlantic AWB activity identified along the +2-PVU contour on the 350-K isentrope. This is consistent with previous studies that identified peak anomalies on or around 350 K (Postel and Hitchman 1999; Abatzoglou and Magnusdottir 2006; Homeyer and Bowman 2013). Homeyer and Bowman (2013) and Kunz et al. (2015) further explained that equatorward AWB tends to occur in regions of weak mean westerly winds resulting from a weakening and a poleward shift of the subtropical jet over the North Atlantic. The increase in AWB activity is

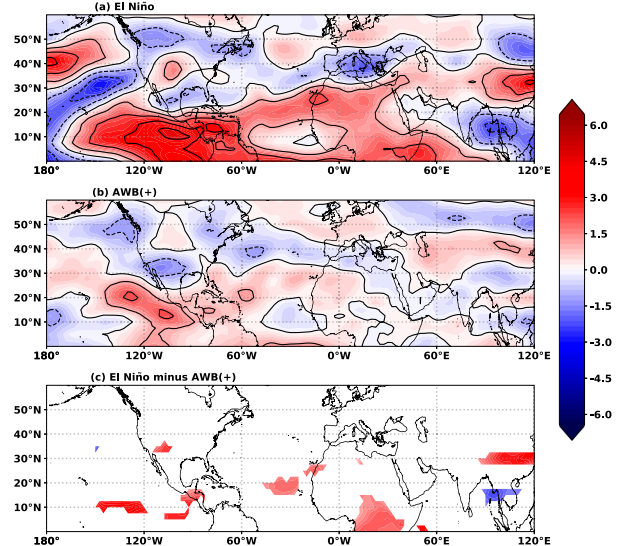


FIG. 3. Comparison of the July–September zonal VWS composites in m s^{-1} for (a) the 12 warmest El Niño seasons vs (b) the 13 most active AWB seasons. Black contours indicate shear anomalies at 2 m s^{-1} intervals. Years used for the El Niño composite are 1982, 1986, 1987, 1990, 1991, 1993, 1994, 1997, 2002, 2004, 2009, and 2015; years used in the AWB(+) composite are 1982, 1985, 1986, 1993, 1994, 2000, 2001, 2003, 2007, 2009, 2011, 2013, and 2014.

also collocated with mean northerly meridional shear (not shown).

To maximize the relationship with tropical VWS and subtropical AWB activity, we focus on the July–September season since this is when AWB shows a distinct peak. In the subsection below, we compare the dynamical variations in July–September VWS influenced by ENSO with variations associated with AWB activity.

b. Spatial variability in VWS composites

Figure 3 shows composites of July–September North Atlantic VWS anomalies in years associated with the 12 warmest El Niño events versus the 13 years with the most intense AWB activity [AWB(+)]. For AWB, our choice of years is based on the PVI index outlined in section 2c; the years chosen are consistent with those identified by Zhang et al. (2016) and Papin et al. (2020). During the warmest El Niño seasons (shown in Fig. 3a), VWS is enhanced over the Atlantic MDR. A similar pattern in the VWS anomaly field is observed in years of intense AWB (Fig. 3b). The difference between the composites (Fig. 3c) shows that ENSO dominates tropical VWS variability. The most significant differences between AWB and ENSO on VWS (assessed using the signed rank test) occur between 20° and 35°N .

Based on separate EOF analyses of mean July, August, and September VWS anomalies, we find that both July

and September have AWB patterns for their second leading monthly modes, similar to those for August. This is consistent with the findings of Zhang et al. (2016), who conducted a similar EOF analysis for the North Atlantic environment in August. We further suggest that the effects of AWB on the Atlantic environment, and consequently TC activity, may also be observed not only in August but in July and September as well. The August composites (not shown) show similar features to the July–September composites, with a pronounced stretch of westerly shear associated with anomalously warm SSTs driven by El Niño. The anomalously strong subtropical jet stream, just north of the African Sahel, is also more evident in the August composites. However, there are few areas with significant differences between the August El Niño and AWB composites within the North Atlantic region.

In Fig. 4, the shear anomaly composite for the 12 coldest La Niña years is compared with a composite of the 13 years with the least intense AWB activity [AWB(−)]. Figure 4 composites show a similar but opposite effect on VWS from those in Fig. 3. As expected, there is very little difference between the La Niña and AWB(−) composites shown in Fig. 4c. Unlike the El Niño–AWB(+) composites, the most significant vertical wind shear difference in the La Niña–AWB(−) composite occurs in the North Atlantic north of 35°N.

There is a great deal of overlap between extreme ENSO seasons and AWB activity, as indicated by the years used to create the composites. Further attempts to separate the two effects indicate that the impacts of tropical and subtropical drivers are not completely separable due to strong tropical–subtropical teleconnections, for example, the AMM–NAO relationship (Grossmann and Klotzbach 2009). The VWS field minus the regressed influences of ENSO and the AMM show no significant correlation with the JAS PVSI index (not shown). Similarly, a frequency separation by applying a high-pass filter on the frequency of days shows little evidence of the characteristic wave breaking pattern.

This suggests that the mechanisms of the two drivers are related, and that ENSO may drive part of AWB variability (Lau and Nath 1996; Martius et al. 2008) or that the effects of ENSO and its teleconnections partially overshadow the effects of other possible drivers. Our AWB activity index has a correlation of 0.14 with the Niño-3.4 index. Zhang et al. (2016) and Papin et al. (2020) showed a correlation of approximately −0.4 between ENSO and AWB activity. While ENSO and AWB activity are not strongly correlated, ENSO dominates VWS variability and masks the effect of AWB on VWS anomalies in both Figs. 3 and 4. Also, significant differences in the composites are observed within the

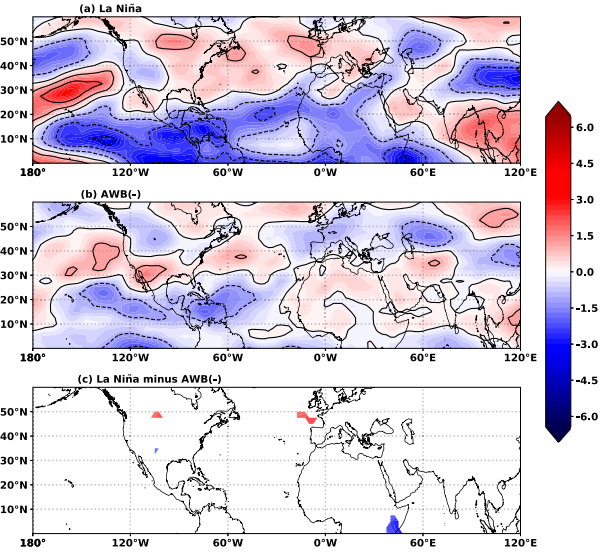


FIG. 4. Comparison of the July–September zonal VWS composites in m s^{-1} for (a) the 12 coldest La Niña seasons vs (b) the 13 least active AWB seasons. Black contours indicate shear anomalies at 2 m s^{-1} intervals. Years used for the La Niña composite are 1985, 1988, 1995, 1998, 1999, 2000, 2007, 2010, 2011, 2016, 2013, and 2017; years used for the AWB(−) composite are 1981, 1987, 1989, 1995, 1997, 1998, 2002, 2004, 2005, 2008, 2010, 2012, and 2016.

Niño-4 region associated with warm pool (WP) ENSO events (Ashok et al. 2007). This may suggest that WP ENSO has a role to play in driving North Atlantic AWB and its effects on tropical VWS. In section 4, we discuss the results of an EOF analysis of mean tropical VWS anomalies to further explore the different effects of ENSO and AWB on VWS in the North Atlantic region. (Note that for the remainder of the study, the abbreviation “EOF” refers to the spatial patterns of the leading modes observed in Fig. 6, while “PC” refers to the principal components or temporal variations associated with each EOF mode, shown in Fig. 7.)

4. Modulation of VWS by AWB in EOFs

a. Eigenanalysis of tropical North Atlantic VWS anomaly

Figure 5 illustrates the variance explained by the first 20 EOFs of July–September tropical North Atlantic zonal VWS. Most of the structured variability in tropical VWS can be accounted for in the first two EOFs, which together explain ~59% of the explained variance. While EOFs 3 and 4 show some continuity with the tail end of the spectrum (explaining 12% and 8% of the variance, respectively), we believe that EOFs 3 and 4 are sufficiently separated from the remaining EOFs to have some physical significance in explaining VWS variability.

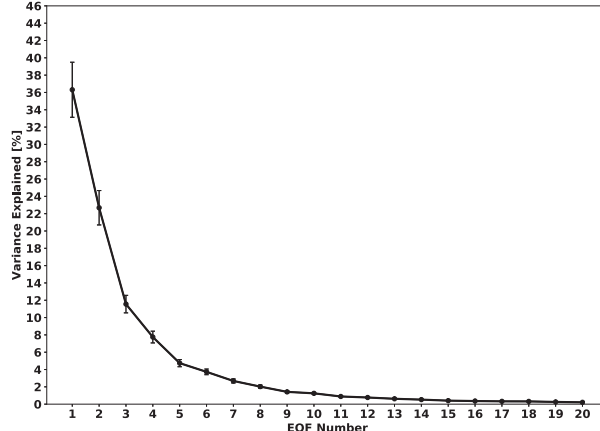


FIG. 5. Spectrum of the covariance matrix showing the percentage variance explained by the first 20 EOFs with the bars representing the 95% error bounds for each EOF. The error distribution of each EOF is calculated using North et al.'s (1982) "rule of thumb."

Based on the criteria outlined by North et al. (1982), we opt to retain the first four EOFs, which together account for 79% of the total variance in zonal VWS in the tropical North Atlantic.

Figure 6 shows a regression of the first four PCs onto July–September global zonal VWS anomalies. The first leading mode of variability (EOF1) shown in Fig. 6a accounts for 36% of the observed variance. The strongest spatial signal, which extends well outside of the North Atlantic region, is mostly confined to the tropical belt and exhibits a tongue-like feature within the Niño-3 region reminiscent of the ENSO signal exhibited in Figs. 3a and 4a and the tropical interannual mode examined in Chelliah and Bell (2004). Correlations with SST anomalies within the four ENSO regions indicate a strong association of temporal variations of EOF1 (PC1) with ENSO variations as shown in Table 2. We note that PC1 shows a significant correlation with all indices used in the analyses. This may be due to PC1 accounting for most of the structured variance in tropical VWS. Variations in both the Walker circulation and Sahel rainfall are known to have teleconnections with equatorial Pacific and Atlantic SST variability (Janicot et al. 1998, 2001). Of the four ENSO indices, the July–September Niño-3.4 index has the strongest correlation with PC1 ($r = 0.73$). PC1 also shows a significant correlation of $r = -0.53$ with the Atlantic meridional mode (AMM). Based on Fisher's r -to- z transformation (Lee and Preacher 2013), the correlation between Niño-3.4 and PC1 is significantly higher than the correlation between the AMM and PC1. This result is expected as ENSO is the dominant driver of tropical interannual variability, and the influence of the AMM–VWS

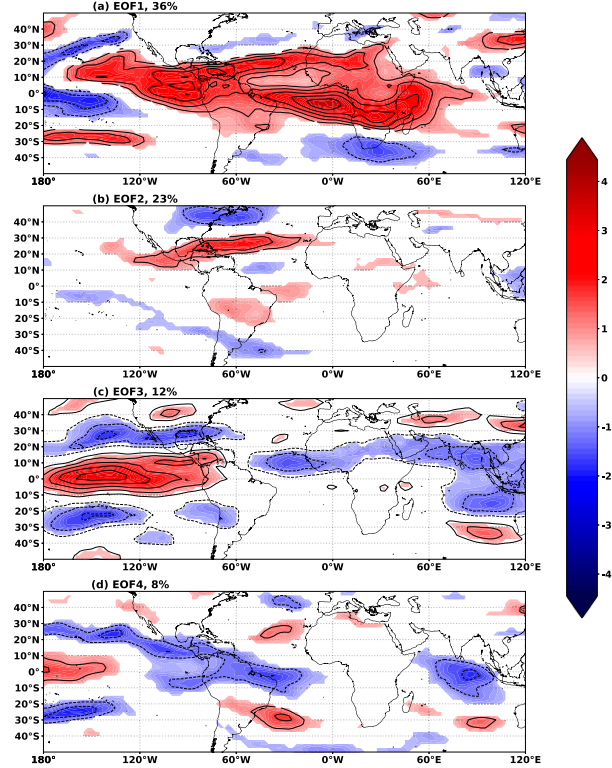


FIG. 6. Regression of the first four principal components onto global zonal VWS anomalies (m s^{-1}). Shaded regions and black contours at 0.5 m s^{-1} intervals indicate standard deviations of $\geq \pm 1$ for westerly (solid) shear anomalies and easterly (dashed) shear anomalies.

relationship is less dominant at high-frequency time scales (Chelliah and Bell 2004; Vimont and Kossin 2007).

Figure 6b displays the second leading mode (EOF2), which accounts for 23% of the structured variance. The EOF2 pattern shows a locally confined lobe of westerly shear (positive zonal anomalies) sandwiched between regions of easterly shear (negative zonal anomalies)

TABLE 2. Pearson correlation between the four leading principal component (PC) time series of tropical North Atlantic VWS with ENSO, PVSI, Sahel, and AMM indices. Correlations statistically significant (based on the two-tailed p value) are highlighted in italics. The strongest correlation with each PC is highlighted in bold.

Index	VWS	PC1	PC2	PC3	PC4
Niño-1+2	0.46	0.54	-0.13	0.42	-0.11
Niño-3	0.65	0.69	-0.02	0.37	-0.09
Niño-3.4	0.73	0.73	0.10	0.29	-0.09
Niño-4	0.73	0.63	0.27	0.35	-0.09
Walker index	-0.38	-0.48	0.07	-0.34	0.04
Sahel	-0.41	-0.56	0.07	0.28	-0.33
AMM	-0.49	-0.53	-0.20	-0.12	0.17
AWB-VWS	0.57	0.43	0.53	-0.01	-0.21

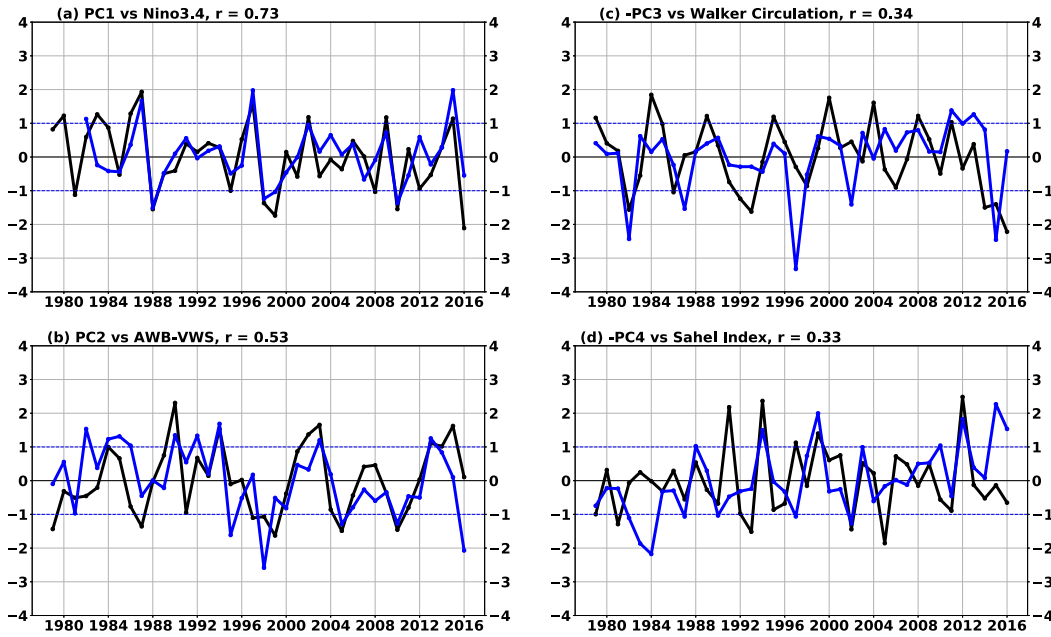


FIG. 7. The first four principal components (PC) of July–September tropical North Atlantic zonal VWS anomalies. The PCs are expressed as a unit variance from the zero mean. Each PC (in black) is plotted along with the July–September climate index (in blue) showing the largest correlation with the PC. PC3 and PC4 are multiplied by a factor of -1 to better highlight the correlation between the corresponding climate index. The Walker circulation and Sahel rainfall indices are standardized to be comparable to PC3 and PC4. The blue dashed lines indicate ± 1 standard deviation.

stretching across the North Atlantic region. EOF2 exhibits features associated with active subtropical wave breaking that have been identified in zonal anomalies by Homeyer and Bowman (2013) and Zhang et al. (2016). In contrast to PC1, correlations with the tropical indices outlined in Table 2 are substantially reduced for PC2, further suggesting that the driver of the second mode of variability is subtropical in nature. AWB activity spurs anomalous easterly shear over the northernmost section of the tropical Atlantic with westerly VWS in the southernmost section of the Atlantic MDR as shown in Fig. 3b. Therefore, AWB(+) years are indicated by strong positive anomalies within the PC2 time series. It is also notable that AWB-associated shear shows a correlation of $r = 0.43$ with PC1. We expect that PC1 will capture much of the variability in tropical VWS including impacts from AWB activity. ENSO and the AMM may also be indirect drivers of AWB activity by modulating large temperature gradients and driving large-scale features such as the Walker and Hadley circulations and thereby triggering AWB (Matthews and Kiladis 1999; Papin et al. 2020; Zavadoff and Kirtman 2019; Zhang and Wang 2019).

EOF3 in Fig. 6c shows a region with strong westerly VWS anomalies, flanked to the north and south by anomalous easterly shear in the equatorial eastern

Pacific region, indicative of an anticyclonic circulation. This strong westerly shear anomaly extends into the western North Atlantic region, while the eastern North Atlantic region is affected by anomalous easterly shear. We hypothesize that the EOF3 pattern is related to the tropical North Atlantic VWS's response to variations in the Walker circulation. The third principal component (PC3) has a correlation of -0.34 with the Walker circulation index (see Table 2). Also, Arkin (1982) found that the anticyclonic pattern shown in EOF3 was generally associated with a warm ENSO phase and a weak phase of the Walker circulation. PC3 also shows a moderate relationship with North Atlantic SSTs (Fig. 8c), which is not surprising given its relationship to anomalous variations in the Walker circulation (Fig. 7c). We further point out that for PC3, the North Atlantic drives the pressure gradient shown in Fig. 9c and may indicate the possible role of the state of the equatorial Pacific relative to the tropical North Atlantic in modulating North Atlantic VWS variability.

The fourth leading mode (EOF4), shown in Fig. 6d, features a tongue of anomalous zonal shear extending from the African Sahel into the tropical North Atlantic MDR. Figure 6d shows easterly shear with a wetter-than-normal Sahel, consistent with the studies of Karnauskas and Li (2016) and Dunion (2011)

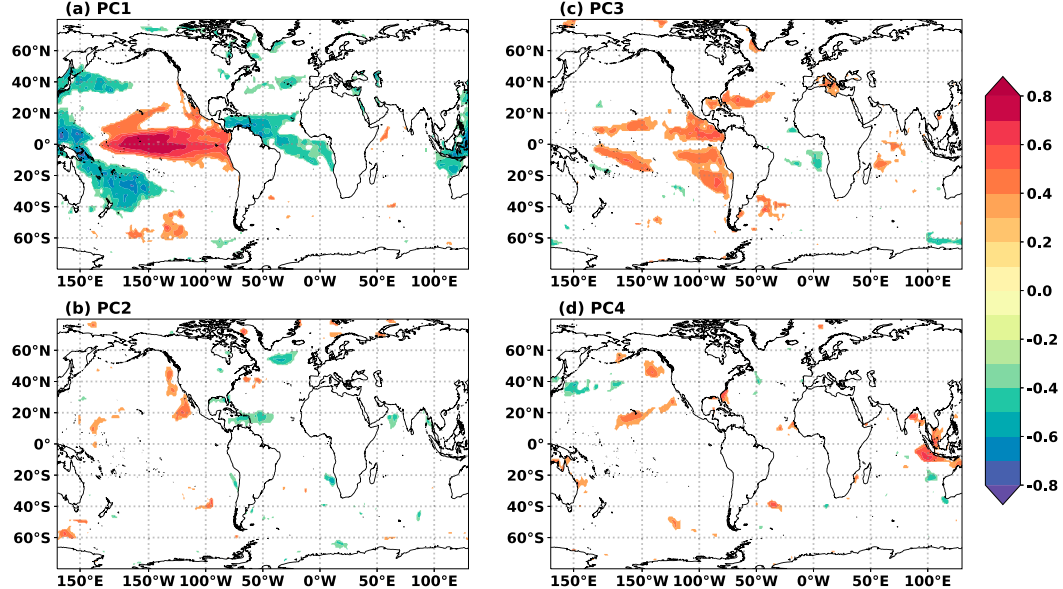


FIG. 8. Spatial Pearson correlations of the first four principal components (PC1, PC2, PC3, and PC4) of tropical North Atlantic VWS with global mean sea surface temperatures. Colored shading indicates correlations statistically significant at the 95% level.

that highlighted the role of Sahel dynamics in influencing the tropical North Atlantic environment. EOF4 explains 8% of the variability in zonal shear in the North Atlantic region. African Sahel rainfall may contribute more to variations in meridional shear as rainfall over Africa is often modulated by a north–south shift of the ITCZ. A wetter-than-normal Sahel induces anomalously

easterly 200-hPa winds (resulting in anomalous easterly shear) while drought-like conditions over the Sahel favor westerly 200-hPa zonal wind and shear anomalies (Zhang and Delworth 2006). Therefore, tropical VWS has an inverse relationship with Sahel rainfall ($r = -0.41$; as shown in Table 2). This is mirrored in correlations between PC4 and Sahel rainfall ($r = -0.33$).

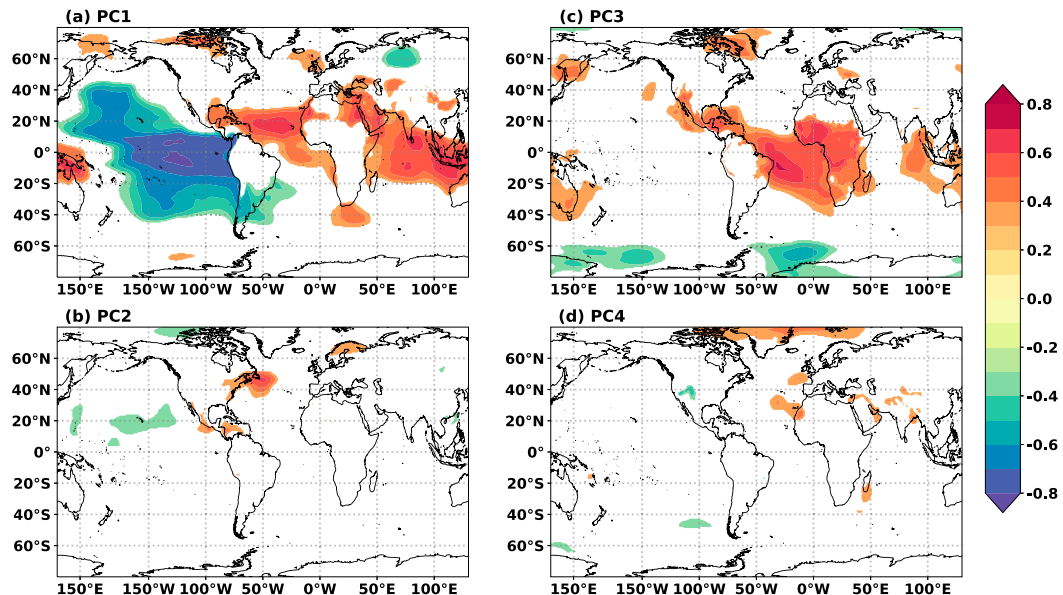


FIG. 9. As in Fig. 8, but for global mean sea level pressure. Colored shading indicates correlations statistically significant at the 95% level.

We note here that the AWB signal featured in EOF2 does not appear in EOF analyses of VWS averaged over the Atlantic MDR generally defined by the area 10° – 20°N , 80° – 20°W . In the EOFs formed from MDR VWS, more than 50% of the explained variance is accounted for by the leading mode of variability and ENSO. African Sahel rainfall is also identified as a major driver, consistent with [Goldenberg and Shapiro \(1996\)](#) and [Aiyer and Thorncroft \(2006\)](#). Our results suggest that variability between 20° and 30°N is necessary to fully capture the impacts of AWB on VWS.

b. AWB-associated VWS anomaly (AWB-VWS) as a predictor of summertime shear

Various studies show that the environmental impact of AWB events can be observed in the modulation of deep-layer VWS ([Zhang et al. 2016](#); [Papin et al. 2020](#); [Li et al. 2018](#)). We create an index of the sum of the shear anomalies collected along the downstream edge of potential vorticity streamers, which is the edge most associated with an increase in westerly shear in the North Atlantic MDR ([Papin et al. 2020](#); [Zhang et al. 2017](#)). The index, referred to as AWB-VWS, shows AWB(+) years to have positive (westerly) anomalies within the North Atlantic, while AWB(–) years show negative (easterly) anomalies, indicating a weak downstream anticyclonic circulation. The AWB-VWS index shows a strong positive correlation with tropical VWS and its first and second modes of variability, consistent with our dynamical explanations of EOF1 and EOF2. As shown in [Table 2](#), AWB-VWS has a 0.57 correlation with tropical North Atlantic VWS anomalies and a 0.53 correlation with PC2. Therefore, EOF2 is strongly influenced by the large easterly shear anomalies lining the northern edge of the tropical North Atlantic region (see [Fig. 6b](#)).

[Table 3](#) outlines the correlations of the time series of PCs1–4 and the AWB-VWS index with seasonal tropical North Atlantic shear and ACE south of 35°N . As expected, PC1 shows the strongest correlations with JAS VWS, but also shows strong correlations with shear prior to and after the shear's peak in the JAS season. Correlations with PC2 are weak prior to JAS and show little correlation with tropical VWS in SON. This is also reflected in correlations with the AWB-VWS index and suggests that AWB activity has the greatest impact on contemporaneous seasonal shear anomalies. This relationship was also observed for subseasonal modulations of shear by AWB activity ([Li et al. 2018](#)). Compared to PC2, the AWB-VWS index shows a stronger correlation with shear outside of the contemporaneous shear season. Correlations with PC3 and PC4 are weaker than the PC1, PC2, and AWB-VWS indices. PC3 has stronger correlations with shear in the August–October and

TABLE 3. Correlations of the four principal components (PC1, PC2, PC3, PC4) and the AWB-VWS index with seasonal tropical North Atlantic VWS and North Atlantic ACE south of 35°N . Correlations statistically significant at the 95% level are highlighted in bold.

	PC1	PC2	PC3	PC4	AWB-VWS
JJA VWS	0.82	0.35	−0.13	−0.08	0.48
JAS VWS	0.86	0.40	−0.14	−0.16	0.57
ASO VWS	0.72	0.35	−0.31	−0.08	0.53
SON VWS	0.45	0.09	−0.40	−0.23	0.18
JJA ACE	−0.30	−0.29	−0.23	0.26	−0.49
JAS ACE	−0.46	−0.32	−0.42	0.17	−0.50
ASO ACE	−0.56	−0.26	−0.32	0.16	−0.58
SON ACE	−0.65	−0.21	−0.32	0.11	−0.53

September–November seasons, while PC4 has weak seasonal correlations.

While the second leading mode of variability only accounts for 23% of the explained variance, previous studies ([Papin et al. 2020](#); [Zhang et al. 2016, 2017](#)) have already indicated the likely influence of AWB-associated VWS on seasonal TC activity. We expect that a better understanding of the contribution of each driver to summertime VWS variability will ultimately improve our understanding of the drivers of seasonal TC activity in the North Atlantic. Tropical zonal VWS has a correlation of −0.43 with July–September ACE (see [Table 3](#)). We further examine the ability of the AWB-VWS index as a predictor of TC seasonal variability in [Tables 4](#) and [5](#). [Table 4](#) shows the average number of various metrics of TC activity for years corresponding to the five highest and lowest values for PC1 and PC2. As expected, changes in PC1 show a stronger change in the TC metrics. The PC2–TC relationship is less consistent with only modest changes in the TC metrics.

We further quantify the contribution of PC2 and AWB-VWS to a statistical linear prediction model for ACE based on zonal VWS. The four leading modes are regressed against ACE using stepwise regression, and the contribution of each mode to the regression strength is outlined in [Table 5](#). A major contribution to the regression is indicated by a decrease in the root-mean-square error (RMSE), an increase in the variance explained (r^2), and an increase in the significance of the variance or F statistic of the linear combination. PC1 holds most of the regression strength and is capable of being a standalone predictor. The addition of PCs 2 and 3 further lowers the RMSE, and improves the variance explained, although changes to the F statistic are modest. The F statistic weakens with the addition of PC4. The AWB-VWS index shows similar skill at simulating ACE compared to the PC1–PC2 model combination. While the contribution may be modest, the inclusion of

TABLE 4. The average number of named storms, hurricanes, major hurricanes, and ACE in the five years with the highest (lowest) standardized values for PC1 and PC2.

	PC1, top five	PC1, bottom five	PC2, top five	PC2, bottom five
Named storms	9	14	13	12
Hurricanes	3	8	5	6
Major hurricanes	2	4	1	3
ACE	44.3	142.5	72.4	80.0

AWB impacts on shear into statistical schemes for operational seasonal prediction shows improvement in accounting for years driven predominantly by AWB. In future research, we will analyze the inclusion of the AWB-VWS index in Colorado State University's statistical TC forecast scheme.

Table 5 also shows that PC3 contributes a significant increase to the regression strength against the July–September ACE index, increasing the variance explained from 27% to 44%. Following a similar stepwise regression approach as described above, with PC3 as the only predictor, PC3 explains $\sim 15\%$ of the observed variance with a regression strength of 7.3. Based on these values, the Walker circulation-associated PC3 may not be the most suitable standalone predictor for ACE, but it does seem to explain an important portion of variance not already covered by PC1 and PC2. In contrast to the other PCs, PC3 has a strong tropical eastern Atlantic signal (Fig. 6c), possibly due to SLP variations over the tropical South Atlantic (Fig. 9c). The regression statistics suggest that the PC1 + PC2 + PC3 combination is a strong representation of the overall impact of VWS on seasonal TC variability.

5. Discussion and conclusions

In this study, both tropical and extratropical contributions to the variability of seasonal 200–850-hPa zonal vertical wind shear in the tropical North Atlantic region were identified using compositing and EOF analysis. Major findings of this analysis include the following:

- 1) The first leading mode of variability in tropical North Atlantic zonal VWS accounts for 36% of the structured variance and is driven by interannual variations in ENSO and the AMM, suggesting that tropical sources of shear are the dominant contributor to VWS.
- 2) Anticyclonic wave breaking (AWB) activity is shown to be associated with the second EOF mode and accounts for 23% of the structured variance. While not as strong as ENSO, this extratropical source of shear is a significant contributor to VWS variability and TC activity.

TABLE 5. The root-mean-square error (RMSE), variance explained (r^2), and F statistic associated with the stepwise regression of VWS, AWB-VWS, and the four leading modes against the July–September ACE index.

Combination	RMSE	r^2	F
VWS only	14.30	0.17	8.61
AWB-VWS only	13.74	0.24	12.37
PC1 only	14.35	0.17	8.33
PCs 1 + 2	13.36	0.27	8.09
PCs 1 + 2 + 3	11.75	0.44	10.70
PCs 1 + 2 + 3 + 4	11.88	0.43	7.91

- 3) The third leading mode is associated with the pressure gradient likely modulated by the Walker circulation, accounting for 12% of tropical VWS.
- 4) African Sahel rainfall is associated with the fourth mode of variability in high-frequency variations of tropical North Atlantic zonal VWS, accounting for 8% of the structured variance.

While the leading EOF modes are by design orthogonal, there remain some shared physical relationships between the drivers of each of the four leading modes. As observed in section 3 above, the influence of AWB on VWS activity is difficult to characterize due to ENSO's strong influence on the tropical North Atlantic region (see Figs. 3 and 4). One limitation of the study was the inability to separately analyze the contributions of AWB to tropical VWS variability due to substantial overlap with strong ENSO events. Even if the threshold definitions of ENSO and AWB events are relaxed, there are still not enough samples of anomalous AWB years with neutral ENSO conditions or anomalous ENSO years with neutral AWB conditions to fully differentiate their impacts on the observed environment. The overlap raises a question about how much ENSO imprints on AWB variability and the subsequent relationship with seasonal TC activity. Therefore, a complete separation of the tropical and subtropical influences has not been achieved. The dominance of ENSO may be a key reason for the inability to observe significant impacts of AWB on seasonal TC activity during all years with anomalous AWB, as observed by Li et al. (2018).

The results presented in section 4 suggest that the tropical sources of VWS from ENSO are indeed dominant, but that extratropical sources of VWS from AWB are an important contribution to tropical and subtropical VWS variability and TC activity. The present analysis shows that the second mode of variability of tropical North Atlantic VWS may be attributed to subtropical AWB activity (Galarneau et al. 2015; Zhang et al. 2017). Our results are consistent with Zhang et al. (2016, 2017), who previously highlighted the dynamical role of AWB

in driving seasonal TC variability through modulations of VWS. The current study adds to their findings by quantifying the AWB impact on the tropical North Atlantic VWS relative to ENSO's strong influence on the tropical North Atlantic summertime circulation.

Another key result is the overshadowing of an AWB signal in the leading modes of interannual variability when restricting analyses of unfiltered tropical North Atlantic VWS to only the main development region (MDR). The MDR does not fully encompass the spatio-temporal patterns driving VWS within the North Atlantic region where TCs are prevalent. The MDR domain is large enough to incorporate the impacts of both ENSO and the African Sahel on VWS (Aiyer and Thorncroft 2006), but not the impacts of AWB. Extending the domain to 30°N better captures the full extent of the leading modes of VWS variability that impact TCs.

This study has focused on zonal VWS due to the fact that meridional VWS variability accounts for a smaller portion of the overall horizontal shear variability. There may be impacts from large-scale variations in the Atlantic multidecadal mode (Patricola et al. 2016) that modulate meridional variations in VWS over the wider North Atlantic (Vimont and Kossin 2007). Further analysis of meridional shear variability is recommended for future work.

While recent studies have improved our understanding of the variability of both deep-layer shear and AWB activity, their impacts on TC activity are not well documented and warrant further research. By examining the deep-layer shear directly, we take the first step to assessing the predictability of VWS and quantifying the response of the environment, and consequently TC activity, with respect to each large-scale driver. VWS anomalies induced by AWB activity (AWB-VWS) may be a better indicator of AWB's impacts on VWS compared to directly using the second leading EOF mode as an index. The AWB-VWS index calculated has a significant correlation with both tropical North Atlantic VWS ($r = 0.57$) and seasonal ACE ($r = -0.50$), suggesting its possible use as a predictor in seasonal TC forecasting. The results of this study highlight the importance of AWB in seasonal North Atlantic TC activity in the summertime, in addition to the impacts of ENSO, the Walker circulation, and Sahel rainfall. Future work will further explore the dynamical relationships between large-scale atmospheric and oceanic drivers of tropical climate and VWS variability, and how AWB variability may be further incorporated into forecasts of seasonal TC activity.

Acknowledgments. This research was supported by the Office of Naval Research Award N000141613033,

the Fulbright Foreign Student Program, the Institute of International Education (IIE), and the G. Unger Vetlesen Foundation. Special thanks are given to Philippe Papin for his many insights and to Ben Trabing for his invaluable comments and suggestions in the writing of this paper. We also thank the editor and the three anonymous reviewers who provided us with many helpful comments and suggestions that improved the paper's final form.

REFERENCES

- Abatzoglou, J. T., and G. Magnusdottir, 2006: Planetary wave breaking and nonlinear reflection: Seasonal cycle and interannual variability. *J. Climate*, **19**, 6139–6152, <https://doi.org/10.1175/JCLI3968.1>.
- Aiyer, A. R., and C. Thorncroft, 2006: Climatology of vertical wind shear over the tropical Atlantic. *J. Climate*, **19**, 2969–2983, <https://doi.org/10.1175/JCLI3685.1>.
- Arkin, P. A., 1982: The relationship between interannual variability in the 200 mb tropical wind field and the Southern Oscillation. *Mon. Wea. Rev.*, **110**, 1393–1404, [https://doi.org/10.1175/1520-0493\(1982\)110<1393:TRBIVI>2.0.CO;2](https://doi.org/10.1175/1520-0493(1982)110<1393:TRBIVI>2.0.CO;2).
- Ashok, K., S. K. Behera, S. A. Rao, H. Weng, and T. Yamagata, 2007: El Niño Modoki and its possible teleconnection. *J. Geophys. Res.*, **112**, C11007, <https://doi.org/10.1029/2006JC003798>.
- Barnes, E. A., and D. L. Hartmann, 2012: Detection of Rossby wave breaking and its response to shifts of the midlatitude jet with climate change. *J. Geophys. Res.*, **117**, D09117, <https://doi.org/10.1029/2012JD017469>.
- Bell, G. D., and Coauthors, 2000: Climate assessment for 1999. *Bull. Amer. Meteor. Soc.*, **81**, S1–S50, [https://doi.org/10.1175/1520-0477\(2000\)81\[s1:CAF\]2.0.CO;2](https://doi.org/10.1175/1520-0477(2000)81[s1:CAF]2.0.CO;2).
- Berrisford, P., P. Källberg, S. Kobayashi, D. Dee, S. Uppala, A. Simmons, P. Poli, and H. Sato, 2011: Atmospheric conservation properties in ERA-Interim. *Quart. J. Roy. Meteor. Soc.*, **137**, 1381–1399, <https://doi.org/10.1002/qj.864>.
- Chelliah, M., and G. D. Bell, 2004: Tropical multidecadal and interannual climate variability in the NCEP–NCAR reanalysis. *J. Climate*, **17**, 1777–1803, [https://doi.org/10.1175/1520-0442\(2004\)017<1777:TMAICV>2.0.CO;2](https://doi.org/10.1175/1520-0442(2004)017<1777:TMAICV>2.0.CO;2).
- Chiang, J. C. H., and D. J. Vimont, 2004: Analogous Pacific and Atlantic meridional modes of tropical atmosphere–ocean variability. *J. Climate*, **17**, 4143–4158, <https://doi.org/10.1175/JCLI4953.1>.
- Dee, D. P., and Coauthors, 2011: The ERA-Interim reanalysis: Configuration and performance of the data assimilation system. *Quart. J. Roy. Meteor. Soc.*, **137**, 553–597, <https://doi.org/10.1002/qj.828>.
- Dunion, J. P., 2011: Rewriting the climatology of the tropical North Atlantic and Caribbean Sea atmosphere. *J. Climate*, **24**, 893–908, <https://doi.org/10.1175/2010JCLI3496.1>.
- Galarneau, T. J., R. McTaggart-Cowan, L. F. Bosart, and C. A. Davis, 2015: Development of North Atlantic tropical disturbances near upper-level potential vorticity streamers. *J. Atmos. Sci.*, **72**, 572–597, <https://doi.org/10.1175/JAS-D-14-0106.1>.
- Goldenberg, S. B., and L. J. Shapiro, 1996: Physical mechanisms for the association of El Niño and West African rainfall with Atlantic major hurricane activity. *J. Climate*, **9**, 1169–1187, [https://doi.org/10.1175/1520-0442\(1996\)009<1169:PMFTAO>2.0.CO;2](https://doi.org/10.1175/1520-0442(1996)009<1169:PMFTAO>2.0.CO;2).

- Gray, W. M., 1968: Global view of the origin of tropical disturbances and storms. *Mon. Wea. Rev.*, **96**, 669–700, [https://doi.org/10.1175/1520-0493\(1968\)096<0669:GVOTOO>2.0.CO;2](https://doi.org/10.1175/1520-0493(1968)096<0669:GVOTOO>2.0.CO;2).
- , 1984: Atlantic seasonal hurricane frequency. Part I: El Niño and 30 mb quasi-biennial oscillation influences. *Mon. Wea. Rev.*, **112**, 1649–1668, [https://doi.org/10.1175/1520-0493\(1984\)112<1649:ASHFPI>2.0.CO;2](https://doi.org/10.1175/1520-0493(1984)112<1649:ASHFPI>2.0.CO;2).
- , C. W. Landsea, P. W. Mielke Jr., and K. J. Berry, 1994: Predicting Atlantic basin seasonal tropical cyclone activity by 1 June. *Wea. Forecasting*, **9**, 103–115, [https://doi.org/10.1175/1520-0434\(1994\)009<0103:PABSTC>2.0.CO;2](https://doi.org/10.1175/1520-0434(1994)009<0103:PABSTC>2.0.CO;2).
- Grossmann, I., and P. J. Klotzbach, 2009: A review of North Atlantic modes of natural variability and their driving mechanisms. *J. Geophys. Res.*, **114**, D24107, <https://doi.org/10.1029/2009JD012728>.
- Homeyer, C. R., and K. P. Bowman, 2013: Rossby wave breaking and transport between the tropics and extratropics above the subtropical jet. *J. Atmos. Sci.*, **70**, 607–626, <https://doi.org/10.1175/JAS-D-12-0198.1>.
- Janicot, S., A. Harzallah, B. Fontaine, and V. Moron, 1998: West African monsoon dynamics and eastern equatorial Atlantic and Pacific SST anomalies (1970–88). *J. Climate*, **11**, 1874–1882, <https://doi.org/10.1175/1520-0442-11.8.1874>.
- , S. Trzaska, and I. Poccard, 2001: Summer Sahel–ENSO teleconnection and decadal time scale SST variations. *Climate Dyn.*, **18**, 303–320, <https://doi.org/10.1007/s003820100172>.
- Karnauskas, K. B., and L. Li, 2016: Predicting Atlantic seasonal hurricane activity using outgoing longwave radiation over Africa. *Geophys. Res. Lett.*, **43**, 7152–7159, <https://doi.org/10.1002/2016GL069792>.
- Klotzbach, P. J., and W. M. Gray, 2008: Multidecadal variability in North Atlantic tropical cyclone activity. *J. Climate*, **21**, 3929–3935, <https://doi.org/10.1175/2008JCLI2162.1>.
- , —, 2013: Summary of 2013 Atlantic tropical cyclone activity and verification of authors' seasonal and two-week forecasts. Accessed 30 August 2018, <https://tropical.colostate.edu/media/sites/111/2016/07/2013-11.pdf>.
- , —, and W. Thorson, 2007: Summary of 2007 Atlantic tropical cyclone activity and verification of authors' seasonal and two-week forecasts. 53 pp., <https://tropical.colostate.edu/media/sites/111/2016/07/2007-11.pdf>.
- , M. A. Saunders, G. D. Bell, and E. S. Blake, 2017: North Atlantic seasonal hurricane prediction: Underlying science and an evaluation of statistical models. *Climate Extremes: Patterns and Mechanisms, Geophys. Monogr.*, Vol. 226, Amer. Geophys. Union, 315–328, <https://doi.org/10.1002/9781119068020.CH19>.
- Kossin, J. P., and D. J. Vimont, 2007: A more general framework for understanding Atlantic hurricane variability and trends. *Bull. Amer. Meteor. Soc.*, **88**, 1767–1782, <https://doi.org/10.1175/BAMS-88-11-1767>.
- Kunz, A., M. Sprenger, and H. Wernli, 2015: Climatology of potential vorticity streamers and associated isentropic transport pathways across PV gradient barriers. *J. Geophys. Res. Atmos.*, **120**, 3802–3821, <https://doi.org/10.1002/2014JD022615>.
- Landsea, C. W., and W. M. Gray, 1992: The strong association between western Sahelian monsoon rainfall and intense Atlantic hurricanes. *J. Climate*, **5**, 435–453, [https://doi.org/10.1175/1520-0442\(1992\)005<0435:TSABWS>2.0.CO;2](https://doi.org/10.1175/1520-0442(1992)005<0435:TSABWS>2.0.CO;2).
- , and J. L. Franklin, 2013: Atlantic hurricane database uncertainty and presentation of a new database format. *Mon. Wea. Rev.*, **141**, 3576–3592, <https://doi.org/10.1175/MWR-D-12-00254.1>.
- Lau, N.-C., and M. J. Nath, 1996: The role of the “atmospheric bridge” in linking tropical Pacific ENSO events to extratropical SST anomalies. *J. Climate*, **9**, 2036–2057, [https://doi.org/10.1175/1520-0442\(1996\)009<2036:TROTBI>2.0.CO;2](https://doi.org/10.1175/1520-0442(1996)009<2036:TROTBI>2.0.CO;2).
- Lee, I., and K. Preacher, 2013: Calculation for the test of the difference between two dependent correlations with one variable in common [computer software]. <http://quantpsy.org/corrtest/corrtest2.htm>.
- Li, W., Z. Wang, G. Zhang, M. S. Peng, S. G. Benjamin, and M. Zhao, 2018: Subseasonal variability of Rossby wave breaking and impacts on tropical cyclones during the North Atlantic warm season. *J. Climate*, **31**, 9679–9695, <https://doi.org/10.1175/JCLI-D-17-0880.1>.
- Martius, O., C. Schwierz, and M. Sprenger, 2008: Dynamical tropopause variability and potential vorticity streamers in the Northern Hemisphere—A climatological analysis. *Adv. Atmos. Sci.*, **25**, 367–380, <https://doi.org/10.1007/s00376-008-0367-z>.
- Matthews, A. J., and G. N. Kiladis, 1999: Interactions between ENSO, transient circulation, and tropical convection over the Pacific. *J. Climate*, **12**, 3062–3086, [https://doi.org/10.1175/1520-0442\(1999\)012<3062:IBETCA>2.0.CO;2](https://doi.org/10.1175/1520-0442(1999)012<3062:IBETCA>2.0.CO;2).
- McIntyre, M. E., and T. Palmer, 1983: Breaking planetary waves in the stratosphere. *Nature*, **305**, 593–600, <https://doi.org/10.1038/305593a0>.
- Mitchell, T., 2013: Sahel precipitation index (20°–10°N, 20°W–10°E), 1901–2017. Joint Institute for the Study of the Atmosphere and Ocean, <https://doi.org/10.6069/H5MW2F2Q>.
- Nolan, D. S., and M. G. McGauley, 2012: Tropical cyclogenesis in wind shear: Climatological relationships and physical processes. *Cyclones: Formation, Triggers and Control*, Nova Science Publishers, 1–36.
- North, G. R., T. L. Bell, R. F. Cahalan, and F. J. Moeng, 1982: Sampling errors in the estimation of empirical orthogonal functions. *Mon. Wea. Rev.*, **110**, 699–706, [https://doi.org/10.1175/1520-0493\(1982\)110<0699:SEITEO>2.0.CO;2](https://doi.org/10.1175/1520-0493(1982)110<0699:SEITEO>2.0.CO;2).
- Papin, P. P., L. F. Bosart, and R. D. Torn, 2020: A feature-based approach to classifying summertime potential vorticity streamers linked to Rossby wave breaking in the North Atlantic basin. *J. Climate*, <https://doi.org/10.1175/JCLI-D-19-0812.1>, in press.
- Patricola, C. M., P. Chang, and R. Saravanan, 2016: Degree of simulated suppression of Atlantic tropical cyclones modulated by flavour of El Niño. *Nat. Geosci.*, **9**, 155–160, <https://doi.org/10.1038/ngeo2624>.
- Postel, G. A., and M. H. Hitchman, 1999: A climatology of Rossby wave breaking along the subtropical tropopause. *J. Atmos. Sci.*, **56**, 359–373, [https://doi.org/10.1175/1520-0469\(1999\)056<0359:ACORWB>2.0.CO;2](https://doi.org/10.1175/1520-0469(1999)056<0359:ACORWB>2.0.CO;2).
- Reynolds, R. W., N. A. Rayner, T. M. Smith, D. C. Stokes, and W. Wang, 2002: An improved in situ and satellite SST analysis for climate. *J. Climate*, **15**, 1609–1625, [https://doi.org/10.1175/1520-0442\(2002\)015<1609:AIHAS>2.0.CO;2](https://doi.org/10.1175/1520-0442(2002)015<1609:AIHAS>2.0.CO;2).
- Saunders, M., and A. Lea, 2014: Summary of 2013 Atlantic tropical cyclone season and verification of authors' seasonal forecasts. Tropical Storm Risk. Accessed 30 August 2018, <http://tropicalstormrisk.com/docs/TSRATL2013Verification.pdf>.
- Strong, C., and G. Magnusdottir, 2008: How Rossby wave breaking over the Pacific forces the North Atlantic Oscillation. *Geophys. Res. Lett.*, **35**, L10706, <https://doi.org/10.1029/2008GL033578>.
- Thorncroft, C., B. Hoskins, and M. McIntyre, 1993: Two paradigms of baroclinic-wave life-cycle behaviour. *Quart. J. Roy. Meteor. Soc.*, **119**, 17–55, <https://doi.org/10.1002/qj.49711950903>.

- Trenberth, K., and Coauthors, Eds., 2020: The Climate Data Guide: Niño SST indices (Niño 1+2, 3, 3.4, 4; ONI and TNI). NCAR, accessed 30 March 2020, <https://climatedataguide.ucar.edu/climate-data/nino-sst-indices-nino-12-3-34-4-oni-and-tni>.
- Vimont, D. J., and J. P. Kossin, 2007: The Atlantic meridional mode and hurricane activity. *Geophys. Res. Lett.*, **34**, L07709, <https://doi.org/10.1029/2007GL029683>.
- Wang, C., 2004: ENSO, Atlantic climate variability, and the Walker and Hadley circulations. *The Hadley Circulation: Present, Past and Future*, Springer, 173–202, https://doi.org/10.1007/978-1-4020-2944-8_7.
- , Z. Song, F. Qiao, and S. Dong, 2010: What signals are removed and retained by using an anomaly field in climatic research? *Int. J. Oceanogr.*, **2009**, 329754, <https://doi.org/10.1155/2009/329754>.
- Wernli, H., and M. Sprenger, 2007: Identification and ERA-15 climatology of potential vorticity streamers and cutoffs near the extratropical tropopause. *J. Atmos. Sci.*, **64**, 1569–1586, <https://doi.org/10.1175/JAS3912.1>.
- Zavadoff, B. L., and B. P. Kirtman, 2019: North Atlantic summertime anticyclonic Rossby wave breaking: Climatology, impacts, and connections to the Pacific decadal oscillation. *J. Climate*, **32**, 485–500, <https://doi.org/10.1175/JCLI-D-18-0304.1>.
- Zhang, G., and Z. Wang, 2019: North Atlantic Rossby wave breaking during the hurricane season: Association with tropical and extratropical variability. *J. Climate*, **32**, 3777–3801, <https://doi.org/10.1175/JCLI-D-18-0299.1>.
- , —, T. J. Dunkerton, M. S. Peng, and G. Magnusdottir, 2016: Extratropical impacts on Atlantic tropical cyclone activity. *J. Atmos. Sci.*, **73**, 1401–1418, <https://doi.org/10.1175/JAS-D-15-0154.1>.
- , —, M. S. Peng, and G. Magnusdottir, 2017: Characteristics and impacts of extratropical Rossby wave breaking during the Atlantic hurricane season. *J. Climate*, **30**, 2363–2379, <https://doi.org/10.1175/JCLI-D-16-0425.1>.
- Zhang, R., and T. L. Delworth, 2006: Impact of Atlantic multi-decadal oscillations on India/Sahel rainfall and Atlantic hurricanes. *Geophys. Res. Lett.*, **33**, L17712, <https://doi.org/10.1029/2006GL026267>.